Photoemission study of electronic structure of half-metallic ferromagnet shandite $Co_3Sn_2S_2$

M. Holder,[1] Yu.S. Dedkov,[1] A. Kade,[1] H. Rosner,[2] W. Schnelle,[2] A. Leithe-Jasper,[2] R. Weihrich,[3] and S.L. Molodtsov[1,4]

[1] *Institut für Festkörperphysik, Technische Universität Dresden, D-01062 Dresden, Germany*
[2] *Max-Planck-Institut für Chemische Physik fester Stoffe, D-01187 Dresden, Germany*
[3] *Institut für Anorganische Chemie, Universität Regensburg, D-93040 Regensburg, Germany*
[4] *Institute of Physics, St. Petersburg State University, 198904 St. Petersburg, Russia*

(Dated: January 13, 2009)

Surface electronic structure of poly- and single crystalline samples of half-metallic ferromagnet $Co_3Sn_2S_2$ was studied by means of angle-resolved and core-level photoemission. The experiments were performed in temperature regimes both above and below a Curie temperature of 176.9 K. The spectroscopic results are compared to the local-spin density approximation band structure calculations for the bulk samples. It is found that the surface sensitive experimental data are generally reproduced by the bulk computation suggesting that the theoretically predicted half-metallic properties of $Co_3Sn_2S_2$ retain at the surface.

PACS numbers: 71.20.-b, 75.50.-y, 79.60.-i

INTRODUCTION

A concept of 'half-metallic ferromagnets' was introduced by de Groot *et al.* [1] for Heusler alloys that are considered to be highly relevant for spin-dependend manipulation of charge carriers [2]. Spin-polarized band structure calculations for NiMnSb reveal metallic properties for the spin-majority electrons, while the spin-minority states possess a band gap at the Fermi energy (E_F). These theoretical predictions were, however, controversially inspected by spectroscopic experiments. While only 50% spin polarization of the Fermi-energy electrons was measured by spin-resolved photoemission (PE) [3], a spin-resolved inverse PE study shows that the polarization at E_F can approach 100% value [4]. The obtained discrepancy was explained by possible segregation phenomena that may lead to considerable deviations of the surface as compared to bulk stoichiometry [3–5]. On the other hand, due to reduced coordination even stoichiometric surface may exhibit electronic structure that is very different as compared to the bulk one [6]. But driven by miniaturization of electronic devices, in particular electronic structure at the surface as probed by spectroscopic techniques became of highest importance for applications.

A half-metallic ferromagnet behavior was recently predicted by Weihrich and Anusca [7] in shandite $Co_3Sn_2S_2$. From band structure calculation they found that a ferromagnetic transition in this compound is accompanied by the formation of a band gap in the spin-minority direction. Since the Fermi level lies within this gap, $Co_3Sn_2S_2$, that is metallic in non-magnetic state, becomes insulating for spin-minority states at a Curie temperature (T_c) of 176.9 K [8]. From a classification given by Coey and Venkatesan [9] $Co_3Sn_2S_2$ can be assigned to type I_A half-metallic ferromagnets.

Measurements of magnetic susceptibility [8, 10] confirm the results of the bulk band structure calculation. It was found that the ferromagnetism in $Co_3Sn_2S_2$ is rather sensitive to structural deviations what becomes clear substituting Co by Ni. Only a few percents of Ni impurities decrease rapidly T_c in $(Co_{1-x}Ni_x)_3Sn_2S_2$. Above $x \simeq 0.2$ the compound is no more ferromagnetic [10]. This experimental finding is in accordance with band structure calculations performed for $Ni_3Sn_2S_2$ by Weihrich *et al.* [11]. In this shandite, the energy gap in exchange-split transition metal $3d$ states is shifted to higher binding energy (BE) as compared to its position in $Co_3Sn_2S_2$. Thus, the transition to ferromagnetism is suppressed. Another important issue reported in Ref. [7] is the influence of Sn and S atoms on electronic properties of $(Co_{1-x}Ni_x)_3Sn_2S_2$. Although Sn and S originating contributions to valence-band (VB) density of states are negligible, particularly S-Sn-S bonds along (111) direction of the crystals are of high importance for the gap formation.

In this contribution we focus on surface electronic structure of $Co_3Sn_2S_2$. Experimental results measured by means of angle-resolved and core-level PE for single crystals both above and below T_c are compared with the corresponding data taken for polycrystalline samples. The spectroscopic results are compared to the local-spin density approximation (LSDA) bulk band structure calculations performed for the non-magnetic and ferromagnetic configurations. It is found that the rather surface sensitive experimental data are generally reproduced by the bulk computation. An enhancement of the Fermi-energy signal measured below T_c is in accordance with the predicted magnetic band splitting resulting in downward energy shift of the spin-majority bands that were unoccupied in the non-magnetic sample. Spin-polarized spectroscopic experiments are necessary to quantify ex-

pected spin polarization of the Fermi-energy electrons in the surface region of $Co_3Sn_2S_2$.

EXPERIMENTAL AND THEORETICAL DETAILS

Samples

$Co_3Sn_2S_2$ samples were prepared by high temperature synthesis [12]. Stoichiometric amounts of the elements were heated in a sealed quartz tube to 950°C. After two days, the temperature was decreased stepwise, at 500°C the tube was quenched in cold water. Composition, structure and thermal properties of the samples were characterized by X-ray diffraction, scanning electron microscopy (SEM), energy dispersive X-ray diffraction (EDX), differential thermal analysis (DTA) and differential scanning calorimetric (DSC) methods. The structure determination was performed at 298 K on an imaging plate system equipped with an Oxford cryostat system. From the crystalline product, only a single phase was identified that exhibits the composition $Co_3Sn_2S_2$. The determined lattice parameters are in agreement with the literature [12]. Stoichiometric single crystals have been grown from Sn flux.

Photoelectron spectroscopy

High-resolution angle-resolved and core-level PE studies were carried out at the Berliner Elektronenspeicherring für Synchrotronstrahlung (BESSY, beamline UE112-PGM-1) and in the laboratory of the Dresden University of Technology. The measurements were performed in ultra-high vacuum (UHV) systems consisting of two distinct chambers for preparation and analysis. The PE spectra ($h\nu$ = 21.2 eV, 40.8 eV, 70 eV, 200 eV, 880 eV, and 1486.6 eV [Al K_α]) were recorded with 180 ° hemispherical electron-energy analyzers (PHOIBOS 150 at BESSY and Scienta 2002 in the laboratory) with energy resolution of 150 meV and 400 meV full width at half maximum (FWHM) in the photon-energy region below 200 eV and above 880 eV, respectively. The angle-resolved PE data in the region of the Fermi energy were analyzed applying deconvolution with a Gaussian accounting for the finite experimental resolution. The measured S 2*p* core-level PE spectra were simulated exploiting the Win-Fit program [13]. PE peaks originating from S atoms in different chemical environments were least-squares fitted with Voigt-shaped subspectra superimposed by step-like integral background.

The analyzers were fixed, while the vertically positioned $Co_3Sn_2S_2$ samples were rotated changing the incidence angle of photons as well as the polar angle of emitted photoelectrons. In order to get clean sample surfaces as necessary for PE experiments the single crystalline species were cleaved *in situ* by means of ceramic or metallic sticks glued at the crystal surfaces in a vacuum better than 3×10^{-10} mbar. The polycrystalline samples were scraped with a diamond file at a pressure better than 8×10^{-10} mbar. Base pressure during the measurements was always in the range of 1×10^{-10} mbar. The samples were studied at room temperature and 40 K that is above and below T_c.

Surface contaminations were monitored by tracing C and O 1*s* core-level signals in photoemission spectra of the species. The Fermi-level energy position of the analyzers were calibrated applying copper polycrystalline foils in electrical contact with the samples.

Band structure calculation

Band structure calculations were performed using the full-potential local-orbital minimum basis code FPLO (version 5.00-19, Ref. [14]) within the local spin-density approximation. In the scalar relativistic calculation the exchange and correlation potential of Perdew and Wang [15] was employed. A basis set was constructed from a combination of Co 3*s*, 3*p* and Sn 4*s*, 4*p*, 4*d* semi-core states as well as Co 4*s*, 4*p*, 4*d*, Sn 5*s*, 5*p*, 5*d* and S 3*s*, 3*p*, 3*d* valence states. All lower lying states were treated fully relativistic as core states. The inclusion of the semi-core states was forced by their non-negligible overlap due to the large extension of their wave functions. The formally unoccupied Sn 5*d* and S 3*d* states were included to improve the completeness of the basis set. The extension of the valence orbitals was controlled by an additional confining potential (r/r_0) with the parameter r_0 optimized with respect to the total energy [16]. A dense mesh of 8000 **k**-points in the Brillouin zone (BZ) has been applied to ensure accurate density of states (DOS) and band structure information. The calculations were carried out for the experimentally determined structural data.

RESULTS AND DISCUSSION

Sample characterization

Surface structure

The crystal structure of the shandite $Co_3Sn_2S_2$ is discussed in detail by Weihrich *et al.* [11]. It is denoted by trigonal-rhombohedral symmetry of space group 166 (R-3m), a lattice parameter a = 5.3754 Å and an axis angle of 59.91 °. According to the trigonal axes, cobalt atoms occupy Wyckoff position 3e, tin atoms are placed in 1a and 1b, and sulfur atoms reside in position 2c with

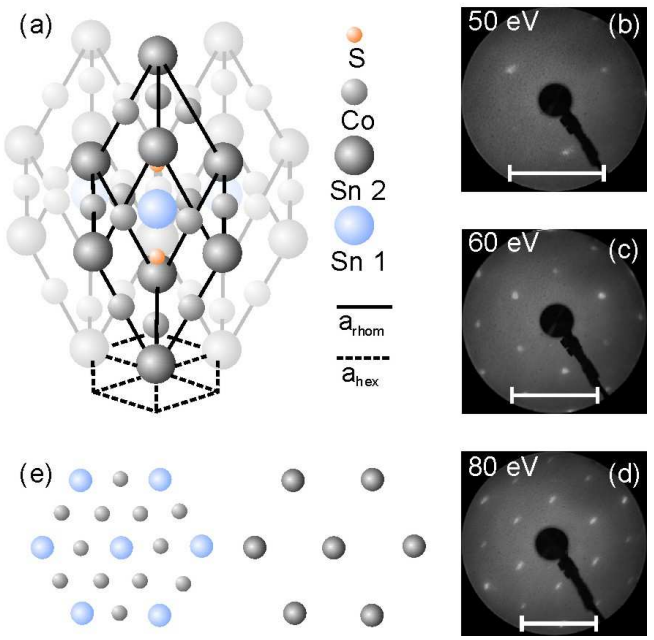

FIG. 1: (Color online) (a) Crystal structure of $Co_3Sn_2S_2$ with rhombohedral basis. Axes of the hexagonal basis are also indicated. (b)-(d) LEED images obtained from (111) surface at different primary electron beam energies. Bars denote scaling of the reciprocal lattice with electron-beam energy. (e) Two possible surface terminations [(i) and (ii), see text] obtained in experiments.

z(S)=0.216. The crystal structure of $Co_3Sn_2S_2$ is displayed in Fig. 1 (a).

Owing to a quasi-layered arrangement of atoms in $Co_3Sn_2S_2$, cleaved surfaces of measured single crystals are always perpendicular to [111] direction. Thus, three surface terminations are possible in the experiment: Sn atoms surrounded by either (i) six Co or (ii) six Sn atoms and iii) S atoms surrounded by six S atoms. Since all (111) planes mentioned above exhibit close packed atomic structures, interpretation of PE spectra in terms of hexagonal symmetry, as indicated in Fig. 1 (a), is justified.

The quality of the surface was checked by low energy electron diffraction (LEED). Obtained sharp images are displayed in Fig. 1 (b)-(d). The hexagonal structure of (111) surface becomes visible at 60 eV and 80 eV primary electron beam energy. Thereby, the intensity of the LEED spots is strongly electron-energy modulated (compare to 50 eV pattern) as expected from the multi-atom basis of the crystal.

Core-level photoemission

To characterize electronic properties of the single crystalline $Co_3Sn_2S_2$ samples first a series of their core levels was measured and compared with corresponding data

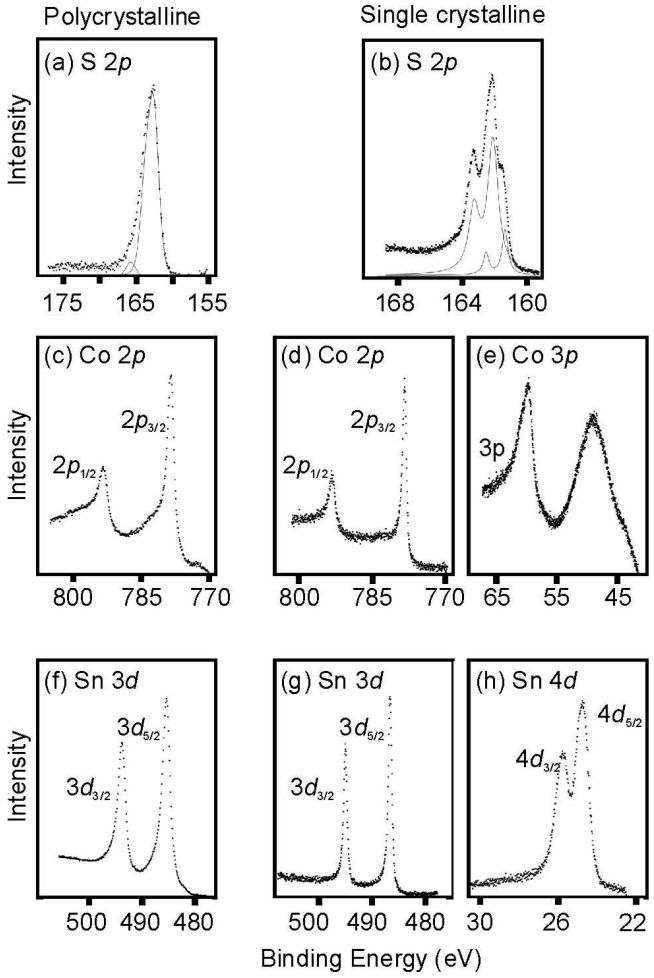

FIG. 2: Core-level PE spectra measured for poly- and single crystalline samples. Results of the least-squares fit analysis are shown by thin lines underneath the S 2p spectra.

taken for polycrystalline species. The core-level PE spectra of the polycrystals were acquired upon Al K_α excitation, while the single crystals were probed with either 200 eV or 880 eV photon energy.

The obtained spectra are shown in Fig. 2. The measured binding energies are compared to results reported in the literature for a number of related compounds in order to gain information about electronic configurations and bonding character in $Co_3Sn_2S_2$. For the isostructural compound $Ni_3Sn_2S_2$, the electronic configuration $(Ni^0)_3(Sn(1)^{2+})(Sn(2)^{2+})(S^{2-})_2$ was derived from Mößbauer and core-level PE experiments [17]. Note, the charge of the S^{2-} ions is completely compensated by the Sn atoms, the Ni atoms remain neutral. A similar situation is expected for $Co_3Sn_2S_2$.

Indeed S^{2-} configuration in $Co_3Sn_2S_2$ is confirmed by measured BE of 162.46 eV for the S 2p state [main component in Fig. 2 (a) and (b)]. In $Co_3Sn_2S_2$, the core level is slightly shifted towards lower binding energy compared to $Ni_3Sn_2S_2$ (162.8 eV) [17]. This shift is not related

to an ionic bonding caused by possible charge transfer from the transition metal to the sulfur. Co may provide one $3d$ valence electron less than Ni and, therefore, the charge density on the sulfur site is expected to be larger in $Ni_3Sn_2S_2$. Thus, the covalent bonding, accompanied by a decrease of the bond length (Ni-S: 2.191 Å, Co-S: 2.178 Å) or different screening of the PE core-hole excitation might cause the observed BE behavior. A similar situation is encountered in transition-metal pyrites. When going from $Co(S^{2-})_2$ to $Ni(S^{2-})_2$ the binding energy of the S $2p$ core level is increased by 0.1 eV [18]. This fact supports the above conclusion that particularly the interplay between the transition-metal and sulfur atoms is responsible for the observed BE variation. In CoS with a S^{2-} configuration the S $2p$ PE signal is found at 169.2 eV binding energy [19]. Here, the S atom is coordinated by 6 Co atoms in a trigonal prismatic arrangement, contrary to antiprismatic configuration in $Co_3Sn_2S_2$.

Besides the discussed above main contribution to the S $2p$ spectra, that is related to the S^{2-} configuration, an additional weak component at 164.5 eV binding energy is found for the polycrystalline samples [see Fig. 2 (a)]. According to Ref. [20] this component stems from S^0 atoms and can be assigned to non-stoichiometric sulfur. For the single crystalline species, apart from the main doublet subspectrum, a second doublet shifted by 0.7 eV to lower BE is monitored [Fig. 2 (b)]. This minor component is interpreted as a surface-derived contribution. The fact that the bulk S subspectrum is characterized by much higher intensity evidences that the cleaved surface is in any case not primarily S terminated. It leaves mainly the (i) and (ii) possibilities for surface termination [Fig. 1 (e)]. Note that the S^0 atoms do not noticeably contribute to the PE intensity in Fig. 2 (b) pointing at good quality of the single crystalline $Co_3Sn_2S_2$ samples measured in the present study.

The binding energy of the Co $2p_{3/2}$ level was measured to be 778.4 eV for both poly- and single crystalline samples [Fig. 2 (c) and (d)]. This value is close to the ones observed in CoS_2 (778.1 eV) and $CoSe_2$ (778.3 eV) and would support a Co^{2+} valence state [18]. In the cobalt lower valent CoSe compound, the Co $2p_{3/2}$ binding energy is 778.7 eV [21]. However, the length of Co-S bonds in $Co_3Sn_2S_2$ indicates covalency. On the other hand, the observed peak separation of 15.1 eV between $2p_{3/2}$ and $2p_{1/2}$ states points at the metallic Co-Sn bonds, contrary to a separation of 16 eV in Co^{2+} compounds. Thus, although pure ionic bonding should be ruled out, the situation is not as clear as in $Ni_3Sn_2S_2$ and some charging of the Co atoms is expected.

Analyzing lineshapes of the Co core-level spectra no satellite structures as reported in Ref. [22, 23] are observed. In these studies the satellite structures were assigned to atomic-like multiplets well known for correlated materials where PE core hole interacts with partly filled localized shells of d or f electrons [24]. This multiplet structure of the $2p_{3/2}$ core level ($\sim$ 778.0 eV BE) was not observed in Co metal [24] pointing at purely itinerant character of $3d$ electrons there. Our data show that also in $Co_3Sn_2S_2$ all valence states are rather extended what justifies our theoretical description of the electronic structure within the LSDA approach. We may assume that the satellite structure measured in Ref. [23] might be related to possible sample oxidation as discussed by Galtayries and Grimblot [24].

The lineshape of the Co $2p$ core-level spectra measured for polycrystalline samples is clearly asymmetric with a tail extending in the region of low binding energies [see Fig. 2 (c)]. This observation can be explained by inelastically scattered photoelectrons and signals stemming from Co atoms occupying non-stoichiometric positions in $Co_3Sn_2S_2$ polycrystals. This asymmetry is strongly reduced in PE spectra measured for the high-quality single crystalline species [Fig. 2 (d)].

From the data obtained by ^{119}Sn Mößbauer spectroscopy in Ref. [17] a valence state 2+ was concluded for the Sn atoms in $Ni_3Sn_2S_2$. Similar measurements done by Weihrich *et al.* [25] on $Co_3Sn_2S_2$ point at partly filled Sn $5s$ shells. In our PE measurements the Sn $4d_{5/2}$ peak in $Co_3Sn_2S_2$ was found at 24.6 eV BE. This energy lies in the range known for Sn chalcogenides ($24.5 - 24.8$ eV, Ref. [26]) and deviates considerably from the value reported for elemental Sn (24.0 eV, Ref. [27]). Oxidation of Sn would shift the $4d$ peak to higher binding energy by about 1.5 eV, as expected for Sn^{2+} configuration. This is not observed in our study both for poly- and single crystalline samples.

The results of the above core-level PE experiments prove extraordinary quality of our samples that are highly suitable for angle-resolved PE studies of the electronic structure of $Co_3Sn_2S_2$ presented below.

Calculated band structure

In the present study, the band structure of $Co_3Sn_2S_2$ was calculated using the approach and the crystalline parameters as described above. The obtained theoretical data are in accordance with the previous calculations of Weihrich and Anusca [7].

Our results, both for the spin-resolved and spin-integrated band structure as well as for corresponding valence-band density of electronic states are shown in Fig. 3. An energy gap between 0.15 eV and 0.45 eV BE is seen in the non-spin polarized calculation. The metallic character of $Co_3Sn_2S_2$ is driven by bands crossing the Fermi energy above this energy gap. In a spin polarization calculation, these bands are split due to exchange interaction. The spin-minority subbands occur above the Fermi energy, while the spin-majority ones shift towards higher binding energies. As a result, the compound becomes insulating for the spin-minority channel, while it

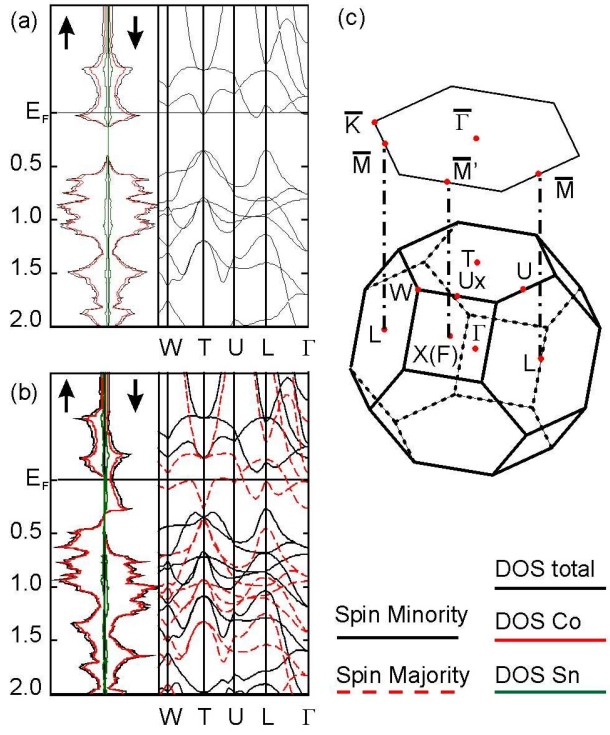

FIG. 3: (Color online) Electronic structure calculated for bulk $Co_3Sn_2S_2$ with (a) unpolarized and (b) polarized spins. (c) Brillouin zone of the compound. Rhombohedral axis intersects the border of the BZ at the L point, while (111) axis crosses it at the T point. The surface projection of the BZ is constructed according to the hexagonal description of the unit cell.

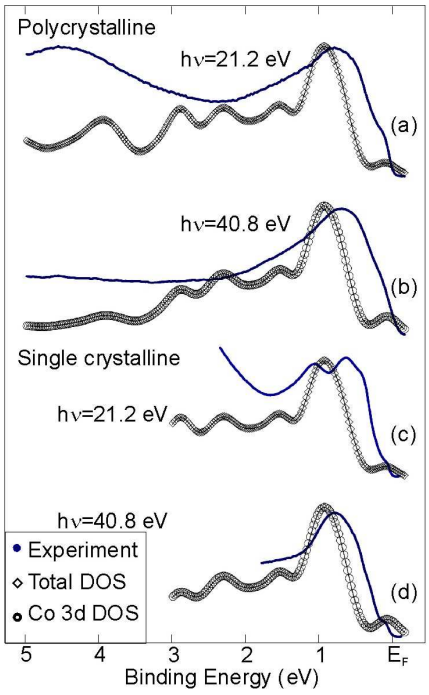

FIG. 4: Angle-integrated valence-band PE spectra of poly- (a,b) and single (c,d) crystalline samples [solid lines] compared with the calculated DOS convoluted with a Gaussian (150 meV, FWHM) [open signs].

remains metallic for the spin-majority direction. The bands around the gap are formed predominantly by Co $3d$ states with a small admixture of Sn and S contributions. Noticeable $5s$ and $5p$ contributions from the Sn atoms lie between 5 eV and 7 eV binding energy. Sn $4d$ states are calculated at about 26 eV BE for both inequivalent positions of these atoms. The calculated magnetic moment is $1\,\mu_B$ per f.u., an integer value as expected for half-metallic ferromagnets [1].

Valence band photoemission

Angle-integrated experiments

Angle-integrated investigation of the VB electronic structure of $Co_3Sn_2S_2$ was performed by means of photoelectron spectroscopy with two different photon energies, $h\nu = 21.2$ eV and 40.8 eV, in order to distinguish in PE signals contributions of electronic states with different angular momentum character. While at $h\nu = 21.2$ eV cross sections of photoionization of Co $3d$ and valence-band p states of Sn and S are characterized by similar values, at $h\nu = 40.8$ eV the Co $3d$ states must cause much higher intensity [28]. The obtained experimental results are compared with our band structure calculations applying the LSDA formalism.

Polycrystals reveal no specific surface orientation. Thus, in contrast to single crystals photoemission of polycrystalline samples provides results that are averaged over different surfaces. Therefore for a given compound, surface specific features can be derived by comparing PE data taken on both types of species. Valence-band spectra acquired for the polycrystalline $Co_3Sn_2S_2$ for 21.2 eV and 40.8 eV photon energies are shown in Fig. 4 (a) and (b). The experimental data depicted in Fig. 4 (c) and (d) are obtained by integration over all measured directions and angles of the angle-resolved spectra taken for single crystalline samples at the same photon energies. In this figure, the experimental results are compared to the calculated total and Co $3d$-projected DOS, convoluted with a Gaussian (150 meV, FWHM), which simulates the finite experimental resolution.

The cross section of the p states drops drastically when going from 21.2 eV to 40.8 eV photon energy. At the same time, the cross section of the Co $3d$ states grows by almost one order of magnitude. Given that independently on photon energy the experimental spectra pre-

sented in Fig. 4 are characterized by resembling lineshapes, only marginal contribution of the p states into the measured energy region of the valence bands is proved then experimentally, in agreement with the theory (Fig. 3). The main partial contribution here stems from the Co 3d states.

Note i) the integrated spectra in Fig. 4 (c) and (d) do not cover as much momentum ($\mathbf{k}$) space as the spectra obtained from the polycrystalline samples and ii) measurements at hν = 21.2 eV and 40.8 eV were performed on different samples, in order to avoid contamination of the surfaces. Thus, distinct surfaces in both single-crystalline measurements cannot be completely ruled out. This might be reflected by the appearance of a double-peak PE structure between 0.4 eV and 1.3 eV BE in Fig. 4 (c) that is not found in Fig. 4 (d) and is not present in the calculated DOS. Apart from this deviation and the finding that the main maxima of the experimental energy distribution curves lie closer to E_F, the experimental data are in general agreement with the calculated DOS. The fact that the main PE peak is located in the close vicinity of the Fermi energy complicates experimental observation

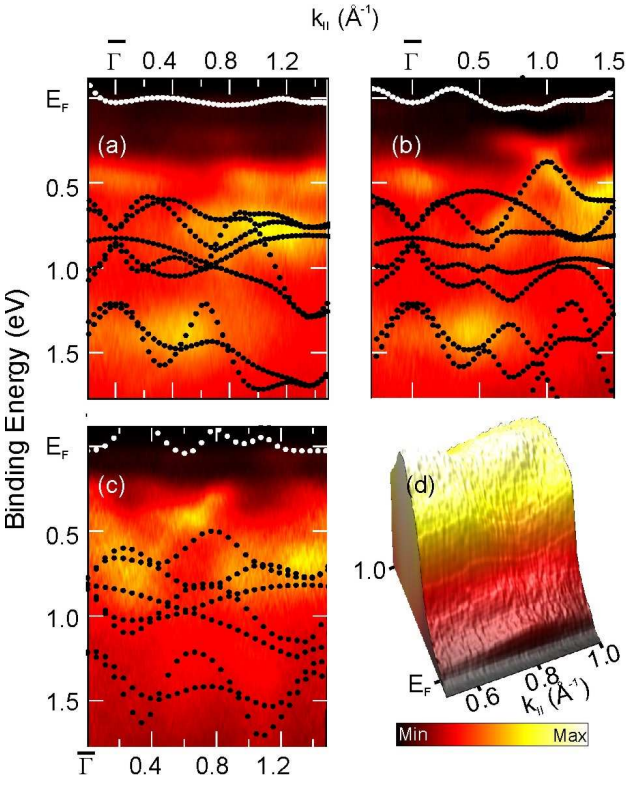

FIG. 5: (Color online) Angle-resolved PE spectra taken at hν = 21.2 eV along the $\bar{\Gamma}$-$\bar{M}$ (a) and $\bar{\Gamma}$-$\bar{K}$ (b) direction as well as at hν = 40.8 eV along the $\bar{\Gamma}$-$\bar{M}$ (c) direction [$\mathbf{k}_{\|}$- momentum vector parallel to the sample surface]. (d) Three dimensional (3D) color plot of PE intensity. Theoretical bands are shown by black (high BE) and white (E_F) dots.

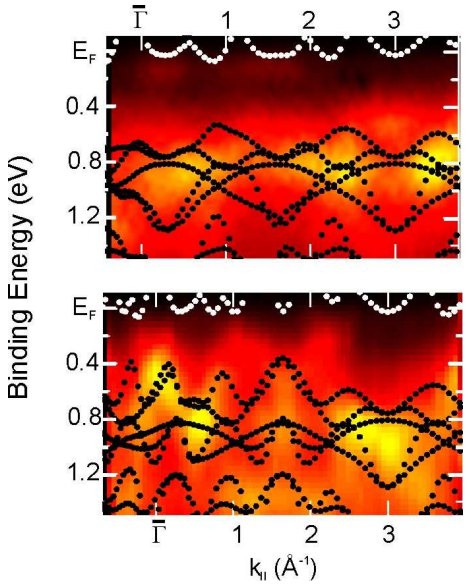

FIG. 6: (Color online) Angel-resolved PE spectra taken at hν = 70 eV along the $\bar{\Gamma}$-$\bar{M}$ direction with linear horizontal (a) and vertical (b) light polarization. Theoretical bands are shown by black (high BE) and white (E_F) dots.

of the energy gap predicted by the theory. The gap between the main peak and the Fermi-energy shoulder can be inferred, however, even from the polycrystalline data, suggesting its formation is not due to only one particular surface termination.

Angle-resolved experiments

A detailed assignment of the calculated non-magnetic band structure to the angle-resolved PE spectra of $Co_3Sn_2S_2$ taken above T_c at room temperature is given in Figs. 5 and 6. The theoretical bands (black and white dots) superimpose the experimental plots (color scale representation) in order to give an estimate for the width of the energy gap and the position of features appearing in the measurements. Three photon energies - 21.2 eV, 40.8 eV, and 70 eV - were used to sample different regions in the BZ. Additionally, variable light polarization (linear vertical and horizontal) was applied for hν = 70 eV in order to follow polarization dependent cross section variations (see Fig. 6).

The momentum vector perpendicular to the surface ($\mathbf{k}_{\perp}$) that is not conserved in photoemission has been evaluated from the free electron model [29]. Thereby the inner potential was first related to the very bottom of the calculated conduction bands and then adjusted to give best agreement with the measured spectra.

In spite of this rather simplified approach to the data interpretation, important correlation between the experimental and theoretical band dispersion can be concluded.

As seen in Figs. 5 and 6 peaks of high intensity between 0.5 eV and 1.0 eV binding energy can be attributed to the dense bunches of the calculated bands. This correspondence was already inferred from our angle-integrated experiments. Note strong light-polarization dependence of the angle-resolved data in Fig. 6 reflecting bands of different symmetries for linear horizontal and vertical light polarization. This shows that non-polarized radiation should necessarily be used to map full electronic structure of $Co_3Sn_2S_2$.

In Fig. 5, features below 0.5 eV binding energy and $\mathbf{k}_{\|} = 0.3\,\text{Å}^{-1}$, $0.8\,\text{Å}^{-1}$, and $1.0\,\text{Å}^{-1}$, respectively, can be particularly well described by the theory. It should be admitted, however, there are some experimental observations that cannot be fully understood based on our single-particle LSDA ground-state calculations and the free-electron like final state model. Namely, the measured energy gap is much smaller than the predicted one and additional PE signals appear above the lower edge of the gap. Electron correlations that are not accounted for in our study might be responsible for the observed discrepancies.

As seen in the 3D plot in Fig. 5 (d) the PE intensity drops drastically when measuring from 0.25 eV BE towards the Fermi level. The signal remaining at E_F might be attributed to a background of scattered electrons. In this case, however, it should appear with nearly constant intensity independently of the region probed in the Brillouin zone. Instead, a detailed data inspection yields weak Fermi-energy intensity modulations at different $\mathbf{k}_{\|}$. In order to increase the contrast, suffering from the low intensity at the Fermi level, the measured spectral lineshapes were deconvoluted with a Gaussian accounting for the finite experimental resolution. By this procedure the Fermi-energy intensity modulations are emphasized and can be assigned to the Fermi-level crossings by the electronic bands that are predicted by our calculations (see Fig. 3).

Despite considerable surface sensitivity of the photoemission experiments, our study reveals good agreement between the measured data and the results of the bulk electronic structure calculations. This conclusion is similar to those drawn from photoemission investigations of high-temperature superconductors where bulk calculations were successfully used for angle-resolved data interpretation as well [30]. This nontrivial finding might be related to the fact that the extended Bloch functions, which describe the bulk electronic states, penetrate with their trailing tails also in the surface region of solids and, therefore, can be probed in photoemission. In any case, our results taken at room temperature make us confident to be able to follow with PE changes of the electronic structure at E_F at temperatures below T_c (176.9 K) predicted by the theory (see Fig. 3).

Corresponding angle-resolved PE spectra taken with $h\nu = 40.8$ eV at $T \sim 40$ K in the range of energies up to 0.5 eV below E_F are depicted in Fig. 7 (a). In Fig. 7 (b) the momentum distribution of the PE intensity along the grey line [marked by arrow in Fig. 7 (a)] is shown by open dots. In this plot the low-temperature $\mathbf{k}_{\|}$ distribution curve (open dots) is compared with the curve acquired at room temperature (solid dots). Since the main differences between results calculated for $Co_3Sn_2S_2$ with unpolarized and polarized spins are seen close to E_F (Fig. 3), the experimental data in Fig. 7 (b) were normalized each point to the PE intensity of the corresponding energy distribution curve integrated between 0.5 eV and 5 eV BE.

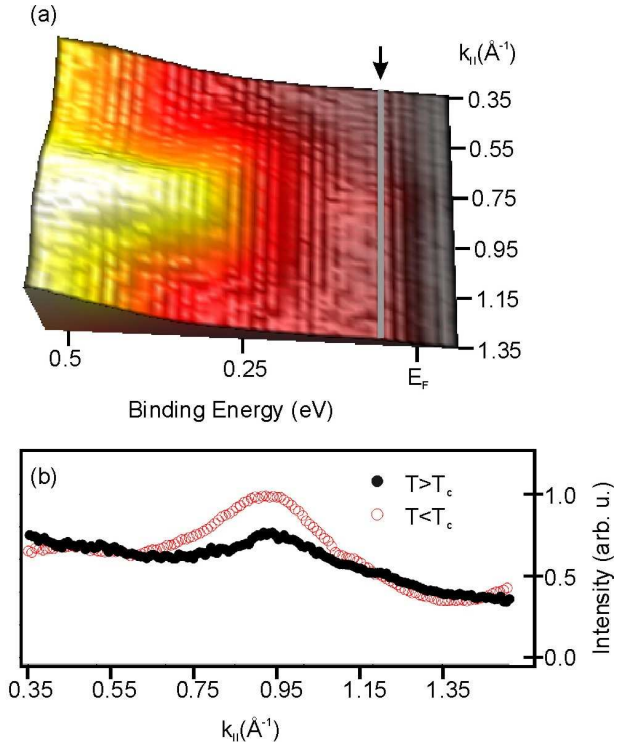

FIG. 7: (Color online) (a) 3D plot of angle-resolved PE intensity close to E_F taken with $h\nu = 40.8$ eV along the $\bar{\Gamma}$-$\bar{K}$ direction in the close vicinity of 40 K. (b) Momentum distribution curves measured at the Fermi energy above (solid dots) and below (open dots) the Curie temperature (see text).

A Fermi-energy signal enhancement at $\mathbf{k}_{\|} = 0.95\,\text{Å}^{-1}$ is clearly monitored in this figure. This result supports the scenario drawn up by our spin-resolved band structure calculations. The spin degeneracy of the Fermi-energy bands that are predicted to stabilize the half-metallic ferromagnetism in $Co_3Sn_2S_2$ is lifted for $T < T_c$: The resulting spin-majority band is shifted far below E_F causing the increase of PE intensity shown in Fig. 7.

CONCLUSIONS

The electronic structure of poly- and single crystalline shandite $Co_3Sn_2S_2$ was studied by means of angle-resolved and core-level PE at the temperatures below and above the Curie temperature. The experimental data are compared with the LSDA band structure calculations carried out both for the spin-unpolarized and -polarized electronic configurations. It is shown that the rather surface sensitive experimental data are reproduced by the bulk computation. The growth of the E_F signal measured below T_c is explained by the lifting of the spin degeneracy at the Fermi level and shifting downwards the spin-majority bands that were unoccupied in the non-magnetic case. Although our present spin-integrated data give strong evidence in favor of the half-ferromagnetic scenario, spin-resolved measurements are necessary to quantify the expected spin polarization of the electrons at the Fermi level in $Co_3Sn_2S_2$.

ACKNOWLEDGMENT

This study was supported by the Deutsche Forschungsgemeinschaft (DFG), projects MO 1049/1-1 and RO 2460/3-1.

[1] A. R. de Groot, F. M. Mueller, P. G. van Engen, and K. H. J. Buschow, Phys. Rev. Lett. **50**, 2024 (1983).
[2] S. A. Wolf, Science **294**, 1488 (2001).
[3] G. L. Bona, F. Maier, M. Taborelli, E. Bucher, and P. H. Schmidt, Solid State Comm. **56**, 391 (1985).
[4] D. Ristoiu, J. P. Nozieres, C. N. Borca, T. Komesu, H.-K. Jeong, and P. A. Dowben, Europhys. Lett. **49**, 624 (2000).
[5] K. E. H. M. Hanssen, P. E. Mijnarends, L. P. L. M. Rabou, and K. H. J. Buschow, Phys. Rev. B **42**, 1533 (1990).
[6] S. J. Jenkins and D. A. King, Surf. Sci. **501**, L185 (2002).
[7] R. Weihrich and I. Anusca, Z. Anorg. Allg. Chem. **632**, 1531 (2006).
[8] R. Weihrich, A. C. Stüeckl, M. Zabel, and W. Schnelle, Z. Anorg. Allg. Chem. **630**, 1767 (2004).
[9] J. M. D. Coey and M. Venkatesan, J. Appl. Phys. **91**, 8345 (2002).
[10] T. Kubodera, H. Okabe, Y. Kamihara, and M. Matoba, Physica B **378**, 1142 (2006).
[11] R. Weihrich, I. Anusca, and M. Zabel, Z. Anorg. Allg. Chem. **631**, 1463 (2005).
[12] M. Zabel, S. Wandinger, and K.-J. Range, Z. Naturforsch. B **34**, 238 (1979).
[13] *Win-fit program:http://www.physik.tu-dresden.de/et/winfit/winfit-install.exe.*
[14] K. Koepernik and H. Eschrig, Phys. Rev. B **59**, 1743 (1999).
[15] J. P. Perdew and Y. Wang, Phys. Rev. B **45**, 13244 (1992).
[16] H. Eschrig, *Optimized LCAO Method and the Electronic Structure of Extended Systems* (Springer, 1989).
[17] P. Gütlich, K.-J. Range, C. Felser, C. Schultz-Münzenberg, W. Tremel, D. Walcher, and M. Waldeck, Angew. Chem. Int. Ed. **38**, 2381 (1999).
[18] H. van der Heide, R. Hemmel, C. F. van Bruggen, and C. Haas, J. Sol. State. Chem. **33**, 17 (1980).
[19] D. C. Frost, C. A. McDowell, and I. Woolsey, Mol. Phys. **27**, 1473 (1974).
[20] D. Briggs and M. P. Seak, *Practical Surface Analysis* (Salle-Sauerfelder, Frankfurt am Main, 1990).
[21] A. B. Mandale, S. Badrinarayanan, S. K. Date, and A. P. B. Sinha, J. Electron. Spectrosc. Rel. Phenom. **33**, 61 (1985).
[22] M. V. Yablonskikh, R. Berger, U. Gelius, R. Lizarraga, T. B. Charikova, E. Z. Kurmaev, and A. Moewes, J. Phys.: Condens. Matter **18**, 1757 (2006).
[23] A. Umetani, E. Nagoshi, T. Kubodera, and M. Matoba, Physica B **403**, 1356 (2008).
[24] A. Galtayries and J. Grimblot, J. Electron. Spectrosc. Rel. Phenom. **98-99**, 267 (1999).
[25] R. Weihrich, F. Schappacher, R. Poettgen, H. Rosner, and W. Schnelle (to be published).
[26] R. B. Shalvoy, G. B. Fischer, and P. J. Stiles, Phys. Rev. B **15**, 1680 (1977).
[27] P. Padova, M. Fanfoni, R. Larciprete, M. Mangiantini, S. Priori, and P. Perfetti, Surf. Sci. **313**, 379 (1994).
[28] J. J. Yeh and I. Lindau, Atomic Data and Nuclear Data Tables **32**, 1 (1985).
[29] F. J. Himpsel, Applied Optics **19**, 3964 (1980).
[30] A. Damascelli, Z. Hussain, and Z.-X. Shen, Rev. Mod. Phys. **75**, 473 (2003).